Journal of
Materials Chemistry C

Accepted Manuscript

Journal of Materials Chemistry C RSCPublishing

ARTICLE

Mechanism of the Reduction and Energy Transfer between Eu^{2+} and Eu^{3+} in Eu-doped $CaAl_2Si_2O_8$ Materials Prepared in Air

Cite this: DOI: 10.1039/xoxxoooooox

Received ooth January 2012,
Accepted ooth January 2012

DOI: 10.1039/xoxxoooooox

www.rsc.org/

W.B. Dai,†[a] Y. F. Lei[b],

Eu^{2+} doped $CaAl_2Si_2O_8$ materials prepared under reducing atmosphere evidence a white-bluish luminescence under UV excitation. Eu^{3+} cations are giving rise naturally to line emission spectra which the colour is between orange and red emissions. To achieve warm color or change the CIE(x,y) position of the $Ca_{1-x}Eu_xAl_2Si_2O_8$ phosphors, we decided to investigate the synthesis of these compounds under air condition to favour co-existence of Eu^{2+} and Eu^{3+} cations and investigate the mechanism of the "abnormal" reduction from Eu^{3+} to Eu^{2+} and the energy transfer from Eu^{2+} to Eu^{3+} in the "co-doped" $CaAl_2Si_2O_8$ host lattice. The results indicate that both Eu^{2+} and Eu^{3+} are co-existing in the aluminosilicates even synthesized under air condition due to the substitution of Eu^{3+} cations for alkaline earth (Ca^{2+}) triggers the formation of $V_{Ca}^{//}$ vacancies that play the role of electron donor towards $Eu_{Ca}^{\bullet}$ defects. The higher the concentration of $V_{Ca}^{//}$, the easier the reduction of Eu^{3+} into Eu^{2+}. Consequently, the "co-doping" with higher state chemical elements (e.g. Zr^{4+}) may help a lot in increasing the concentration of Eu^{2+} cations at the expense of Eu^{3+} ones. For sure, we will take advantages of this observation in the future to prepare materials.

1. Introduction

Due to their luminescent properties, extensive investigations have been devoted to Eu^{2+}-doped luminescent materials. [1-10] In this group of phosphors, aluminates, silicates, aluminosilicates received much attention and some of them give rise now to major applications in plasma display panels or white lighting (e.g. $BaMgAl_{10}O_{17}:Eu^{2+}$, [6] $MAl_2O_4:Eu^{2+}$ (M= Ca, Sr, Ba), [2, 8, 10] $CaMgSi_2O_6:Eu^{2+}$, [7] etc). It is well-known that Eu^{2+} emits a broad band which can span in a large wavelength region ranging from ultraviolet to yellow (and even red) depending on the crystal field strength generated by the surrounding ligands, which depends on their charge, size and the strength of the ligand-to-metal ion bond. Actually, the fluorescence of Eu^{2+} is commonly associated with the Laporte allowed transition $4f^65d^1 \rightarrow 4f^7$ and can be tuned at wish via the proper choice of the host lattice. [3] Eu^{3+} doped materials, e.g. oxides, [11, 12] borates, [13, 14] phosphates, [15] sulfides, [16] are also widely investigated. In contrast with Eu^{2+} cations, the emission of trivalent europium is made up of narrow lines occurring at longer wavelengths (red or orange luminescence) which, in turn, are very useful for application in lighting and display industry (e.g. color TV). [15] These emission lines are mainly associated with transitions from the excited $^5D_0$ level to the ground state ^7F_j (j = 0 to 6) within the $4f^6$ configuration. [17] Furthermore, the transition probabilities of the line emission spectra of Eu^{3+} from $^5D_0$ to the different ground states ^7F_j strongly depend on the symmetry of the site occupied by the activator in the host lattice. [4, 18] Namely, at a site without inversion symmetry, Eu^{3+} will exhibit the hypersensitive forced electric-dipole $^5D_0 \rightarrow {}^7F_2$ transition with emission wavelengths of about 610-620 nm. In contrast, the allowed magnetic-dipole $^5D_0 \rightarrow {}^7F_1$ transition is strongest and usually observed at around 590 nm from Eu^{3+} located at a site with inversion center. Thus, contrary to Eu^{2+} cations, Eu^{3+} activators yield luminescence which is almost not dependent of the host lattice. [19, 20]

During recent decades, the study of resonant energy transfer (ET) between impurity ions has been a famous area mainly because of its importance in the development of efficient phosphor materials (e.g. flat panel displays, [8] radiation detectors, [9] communication devices and solid state lasers [1]). Meanwhile, to our knowledge, the transformation of Eu^{3+} into Eu^{2+} phenomenon in air has been already found in many compounds, such as mixed metal chlorides, [21] oxides, [10] sulphides, [16] under a well crystallized form [22] or as glasses. [23-27] For this study, we are the first to report on the photoluminescence properties of Eu-doped $CaAl_2Si_2O_8$ compounds synthesized in air with the co-existence of Eu^{2+}/Eu^{3+} and ET from Eu^{2+} towards Eu^{3+}. Formally, before any characterization, the co-existence of these two kinds of europium prepared in air can be suspected (Figure 1, excited at two different wavelengths, namely 254 nm and 365 nm with a Fisher Bioblock labosi UV lamp). Pink and white-bluish luminescence is assigned to Eu^{3+} and Eu^{2+} cations, respectively.

Based on these observations, we embarked on the characterization of the $CaAl_2Si_2O_8$: Eu system prepared in air.

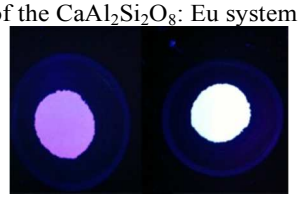

Figure.1 Photographs of $CaAl_2Si_2O_8$: 5%Eu prepared in air excited at 254 nm (pink colour) and 356 nm (white-bluish colour)

2. Experimental section

2.1. Raw materials and synthesis process

Materials were prepared via ceramic route in air with the target $Ca_{1-3x/2}Al_2Si_2O_8$: xEu^{3+} and $Ca_{1-x}Al_2Si_2O_{8+0.5x}$: xEu^{3+} formulations. Precursors were weighted in stoichiometric amounts. Basically, calcium carbonate ($CaCO_3$ 99.997% Alfa Aesar), silica (SiO_2 99.99% Chempur), γ-alumina (Al_2O_3 99.997% Alfa Aesar) and europium oxide (Eu_2O_3 99.99%), were weighted in the appropriate proportions without further purification. Doping rates varied from 0.5 to 13 mol % (except where indicated, all dopant percentage in this study is in mol unit) for the $CaAl_2Si_2O_8$. Starting materials were placed in silicon nitride container 70% filled with ethanol and ball milled with a Fritsch Pulverisette 7 for about two hours to ensure a complete mixture. Then, after drying in an oven at ~ 150°C, blends were calcined at about 1350°C for 50 h under air atmosphere. The air atmosphere is replaced by reducing condition (argon/hydrogen (95/5%)) and the target composition is $Ca_{1-x}Al_2Si_2O_8$: xEu^{2+} when the "only" stabilization of Eu^{2+} cations is desired. To make it simple, hereafter, $CaAl_2Si_2O_8$ sample will be named CASO. In all these materials, the rare earth cations (Eu^{2+}, Eu^{3+}) are expected to substitute for the alkaline earth cations (Ca^{2+}) in the host lattice for steric reasons. [3, 28] Note here when Eu^{3+} cations are inserted in the CASO, we can, *a priori*, envision two different kinds of compositions for our samples to respect the charge balance, namely, the formula of $Ca_{1-3x/2}Al_2Si_2O_8$: xEu^{3+} and $Ca_{1-x}Al_2Si_2O_{8+0.5x}$: xEu^{3+}, respectively (see below in section 3.4).

2.2. Optical measurements

Photoluminescence (PL) and PL excitation (PLE) spectra for all the phosphors were obtained with a Spex Fluorolog-3 spectrofluorometer (Instruments Jobin Yvon) equipped with a 450-W Xe light source and double excitation monochromators. The luminescence decay curve was obtained from a Lecroy Wave Runner 6100 digital oscilloscope (1GHz) using a tunable laser (pulse width = 4 ns, gate = 50 ns) as excitation source (continuum sunlite OPO). The Commission International de I'Eclairage (CIE) chromaticity coordinates for all samples were determined by a Laiko DT-100 colour analyzer equipped with a CCD detector. All of the measurements were performed at room temperature. The spectra decomposition and emission decay fit were accomplished with the Origin8.1 software (originLab Corporation, U.S.A) using Gaussian curves.

2.3. Structure characterizations

The phase purity and crystal structure of the sample were examined by powder X-ray diffraction (XRD) profiles which were measured with a Bruker AXS D8 advanced automatic diffractometer with Cu K-L_3 radiation (germanium monochromator) operated at 40 kV and 40 mA. Furthermore, the structure refinements based on Gebert's crystal investigations [29] are carried out with the Jana2006 Beta version software. [30] The instrumental function was expressed in terms of the geometry of the diffractometer with the relevant parameters which reported in Table 1.

Table 1 Instrumental data Used for Rietveld Refinements of CASO and its Ce^{3+}, Mn^{2+}-doped Derivatives

Primary and second radius	217.5mm
Receiving slit length	16mm
Glancing angle	13.65º
Source and sample length	12mm
Primary soller slit aperture	2.5º
Reception slit divergence angle	0.2º
Receiving slit width	0.1mm
Peak-shape function	Lorentzian

CASO was belonged to triclinic crystal system with space group I-1 [31] which has both layered and framework structure. In the layered structure, the Ca^{2+} ions are located in the interlayers of the double tetrahedral layers and are expected to exchange readily through the interlayers. According to the Wyckoff, CASO structure contains four crystallographically different Ca sites at the same Wickoff position, 4i (Figure 2).

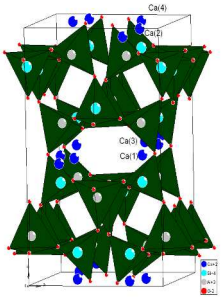

Figure.2 CASO structure represented in cell along the c axic

Due to the requirement of charge neutrality when Eu^{3+} replaced Ca^{2+}, all the four sites are not full occupied and induced the disorder of bond angle and length. According to the occupation of two different chemical sites, we can divide the four Ca^{2+} sites into two groups. Namely, one type of Ca^{2+} ion occupies an octahedral site with six oxygen atoms and the average Ca-O bond distance is 2.485 Å. Other Ca^{2+} ions occupy three kinds of polyhedral sites with seven coordinated oxygen atoms and their average bond distances are 2.508, 2.531, and 2.562 Å, respectively (Figure S1, in supplementary materials). Therefore, the different chemical environment of Ca (Eu) sites in 7- and 6-coordinate number prompted us to think that Eu cations would form two emission centres based on the fact that the higher the coordination of doped cations, the lower the crystal field splitting and the shorter the emission wavelength. [3] Al and Si atoms both occupy tetrahedral sites with four coordinated

oxygen atoms, and the average bond distances for Al-O and Si-O are 1.735 and 1.611 Å, respectively. Because the ionic radii (Pauling's) of Eu^{3+} (r = 0.947 Å when CN = 6, r = 1.05 Å when CN = 7) is much closer to Ca^{2+} (r = 1.00 Å when CN = 6, r = 1.06 Å when CN = 7) since both four coordinated Al^{3+} (r = 0.39 Å) and Si^{4+} (r = 0.26 Å) sites are too small for Eu^{3+} to occupy. Based on the effective ionic radii with different coordination number, [32] it can be proposed that Eu^{3+} (and Eu^{2+}) ions are expected to occupy the Ca^{2+} sites preferably.

The XRD patterns were collected in the 10-90° 2θ range and all the doped samples diffraction peaks are in good agreement with that reported in JCPDS file 89-1462 as exemplified in Figure 3 for x = 5% (under air condition, $Ca_{1-3x/2}Al_2Si_2O_8$). No characteristic peaks of the dopants were observed after a full pattern matching analysis, which means solid-state solutions are formed in all the samples. Note here, the experimental spectrum is not fitted well with the calculate spectrum as shown in Figure 3. This result can be explained by the following: i) powder diffraction was from CASO structure (triclinic, with lower symmetry) which induce overlap of the diffraction peaks and ii) the different radii between Eu^{3+} and Ca^{2+} made the distort of the bond angle and length and iii) lots of holes would be created in the CASO host lattice for the charge balance and many O^{2-} ions may go into the interval of the lattice also caused the bad refinement induced by the different valence between Eu^{3+} and Ca^{2+} ions.

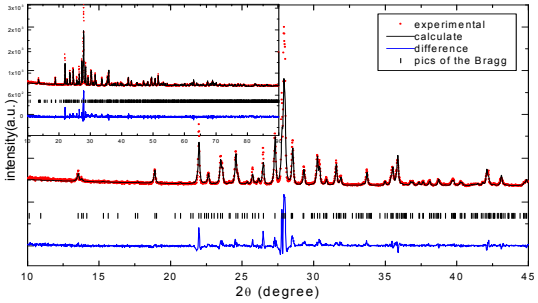

Figure.3 Observed, calculated and difference X-ray diffraction pattern of an Eu^{3+} (0.05)-doped CASO phosphor in the [10-45] 2θ range (inset is given the total pattern)

Meanwhile, the lattice parameters of $C_{1-x}Eu_xAl_2Si_2O_8$ (x = 0 to 70%, synthesized under reducing atmosphere) samples calculated from XRD data are displayed in Figure S2. Due to the ionic radius difference between Eu^{2+} and Ca^{2+}, cell parameters and volume increase with the amount of Eu^{2+} ions. One can see that the solid solution respects the Vegard's law for Eu^{2+} concentration up to a 70% substitution rate. Beyond, the $Ca_{1-x}Eu_xAl_2Si_2O_8$ compound (x > 70%) co-exists with the monoclinic $Eu_{0.92}Al_{1.76}Si_{2.24}O_8$ compound (ICDD # 80-0408). When samples synthesized under air condition, against any expectations, the evolution of lattice parameters with "co-doping" $Eu^{2+/3+}$ cations were also investigated but no significant evolution was found due to: i) majority amount of Eu^{3+} appears in the CASO host lattice and ii) r(Eu^{3+}) similar to r(Ca^{2+}).

3. Results and discussion

3.1. Photoluminescence properties of $C_{1-x}ASO: xEu^{2+}$ (in reducing atmosphere)

The PLE and the PL spectra of the $C_{1-x}Eu_xAl_2Si_2O_8$ samples monitored at λ_{em} = 420 nm and λ_{ex} = 320 nm are displayed in Figure 4. PLE spectrum is composed of a very broad band which can be deconvoluted into two contributions, one centred at around 320 nm, the other at about 287 nm. This absorption band is associated with Eu^{2+}- $4f^7 \rightarrow 4f^65d^1$ electronic transitions where the d block is split due to the ligand field. The intense broad emission bands, located between 420 nm and 475 nm versus the Eu^{2+} concentration, are associated with $4f^65d^1 \rightarrow 4f^7$ ($^8S_{7/2}$) radiative transition of Eu^{2+}. [1, 3] Actually, the broad emission bands are due to the allowed character of the 5d → 4f transitions but also to the existence of two kinds of alkaline earth sites available for the activator. As one can see in Figure 4, the higher the Eu concentration, the longer the emission wavelength is. The red shift could be related to an increasing of the energy transfer from one Eu^{2+} (7-) to another Eu^{2+} (6-) when Eu concentration increases.

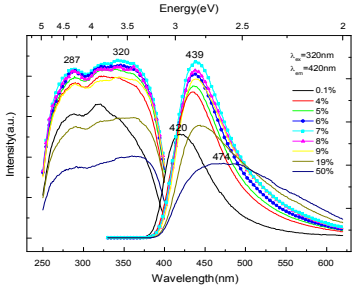

Figure.4 Excitation and emission spectra of $Ca_{1-x}Eu_xAl_2Si_2O_8$ (x = 0.1% to 50%) collected at room temperature, under λ_{ex} = 320 nm and λ_{em} = 420 nm

Let notice that Clabau et al. had detected Eu^{3+} species in this material by Mossbauer spectroscopy, [3] very low intensity of Eu^{3+} cations luminescence emission can be detected. As one can see Figure 5, it illustrates the PL spectrums of CASO: 5%Eu prepared in air and reducing atmosphere, respectively. Obviously, the Eu^{2+} emission intensity (broad band) for the sample prepared under reducing atmosphere is much stronger than the air condition one and the opposite trend is found in the longer wavelength from Eu^{3+} cations emitting. By comparing the spectral characteristics of the emission bands, it can conclude that the reduction $Eu^{3+} \rightarrow Eu^{2+}$ took place when synthesized in air condition. As expected, the lower emission intensity of Eu^{3+} in the sample synthesized under reducing atmosphere is because: i) the 4f-4f emission from the Eu^{3+} cations are forbidden as electric dipole transitions and are several orders of magnitude less intense than the spin and parity allowed 5d → 4f transitions of Eu^{2+}, ii) the contents of Eu^{3+} ions are quite low compared to those of Eu^{2+}, iii) excitation at 320 nm is not well appropriate for favouring the 4f-4f transitions of Eu^{3+}.

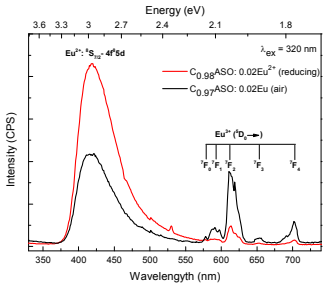

Figure.5 Emission spectra of CASO: 5%Eu prepared in air (black line) and reducing atmosphere (red line) under λ_{ex} = 320 nm

When Eu^{3+} doped at low symmetry site, the predominant transition ($^5D_0 \rightarrow ^7F_2$) of the emission band is located at approximately 610 - 620 nm and this is the case for CASO matrix (Figure 5). Based on this consideration, we also depict the PLE spectra monitored at λ_{em} = 611 nm for the samples $C_{1-x}Eu_xAl_2Si_2O_8$. As observed in Figure S3, two weak 4f-4f absorption peaks located at around 393 and 463 nm can be detected ($^7F_0 \rightarrow ^5L_0$ and $^7F_0 \rightarrow ^5D_2$, respectively). On the basis of these luminescent results and the Mossbauer spectra, [3] we can confirm that both Eu^{2+} (majority) and Eu^{3+} ions co-exist in the CASO matrix even synthesized in reducing atmosphere. It is worthy to note that the spectra shape PLE of $C_{1-x}Eu_xAl_2Si_2O_8$ monitored at 611 nm has a similar appearance than CASO: Eu^{2+} monitored at 420 nm (Figure 4) with characteristic 4f-4f line peaks (at 393 and 463 nm for instance) in addition. Therefore, we can suppose that Eu^{2+} co-doped with Eu^{3+} in the CASO matrix can impact the CIE parameters because of energy transfer (ET) from Eu^{2+} to Eu^{3+} (see below for materials prepared in air).

The decay times of Eu^{2+} cations doped CASO with x ranging from 0.5 to 50% have also been measured. The evolution of the intensities vs. time once excitation stopped is given in Figure 6 according to Equation (1): [28]

$$I = I_0 \exp(-t/\tau)$$

Surprisingly, whatever the substitution rate, the lifetimes associated with the Eu^{2+}- $4f^65d^1 \rightarrow 4f^7$ radiative transition are almost the same, namely, 0.65 µs. This value agrees with data reported in the literature [28, 33] (0.73 µs) and is characteristic of Eu^{2+} cations. At this stage, we can consider that the value of Eu^{2+} decay times is not impacted by the occurrence of ET (from Eu(7-) to Eu(6-)) when Eu concentration increases.

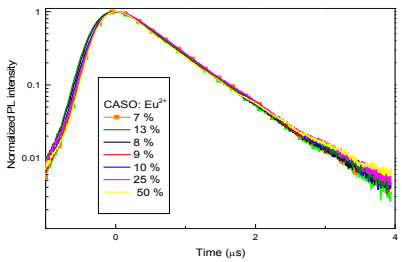

Figure.6 Photoluminescence decay curves of $C_{1-x}Eu_xASO$ (x = 0.5% to 50%, λ_{em} = 420 nm and λ_{ex} = 265 nm)

3.2. Photoluminescence properties of $C_{1-3x/2}ASO$: xEu^{3+} and $C_{1-x}ASO_{8+0.5x}$: xEu^{3+} (0 < x < 13%, in air condition)

Figures S4 shows the PLE and PL of the compounds $C_{1-3x/2}Al_2Si_2O_8$: xEu (x = 0.5% to 13%) synthesized in air condition monitored at typical Eu^{2+} optical transitions, namely, λ_{ex} = 320 nm and λ_{em} = 425 nm. One can see that the PLE spectra monitored at 425 nm shows an optimal excitation 4f → 5d bands centred at 320 nm with a shoulder at 287nm, while the emission band located at around 425nm is due to the typical transition of Eu^{2+}. Then, we can assume that Eu^{2+} ions are present in the CASO when synthesis is even performed in air conditions. Interestingly, the Eu^{2+} emission intensity begins to decrease at the dopant rate about 2% (even if all the Eu cations are in the divalent state), we can suppose that the decreasing of the intensity is due to the ET from Eu^{2+} to Eu^{3+} since the critical concentration for Eu^{2+} in CASO is about 7% (Figure 4).

Figure 7 shows the PLE spectra for Eu-doped CASO, under both formulas and for different Eu concentrations, excitation being monitored at 611 nm corresponding to the predominant transition of Eu^{3+}, namely $^5D_0 \rightarrow ^7F_2$ transition. As one can see, PLE spectra consists of several sharp excitation bands corresponding to the typical intra-4f transitions of Eu^{3+} ions and a $O^{2-} \rightarrow Eu^{3+}$ charge transfer band (CTB) located in the UV range. Here, it is very interesting to notice that the broad CTB overlap with the weaker bands located at about 320 nm for CASO: $Eu^{2+/3+}$. Actually, as mentioned before, the 320 nm band is corresponding to the Eu^{2+} excitation transition. The weak excitation bands of Eu^{2+} indicate not only the presence of Eu^{2+} cations but also the existence of ET from Eu^{2+} ions of 5d level to the Eu^{3+} ions of 4f levels (spectra monitored at 611 nm). The sharp excitation bands relative to the 4f transitions centred at 361, 382, 393, 413, 463, 530 and 576 nm can be attributed to the $^7F_0 \rightarrow ^5D_4$, $^7F_0 \rightarrow ^5L_7$, $^7F_0 \rightarrow ^5L_0$, $^7F_0 \rightarrow ^5D_3$, $^7F_0 \rightarrow ^5D_2$, $^7F_0 \rightarrow ^5D_1$ and $^7F_0 \rightarrow ^5D_0$ transitions, [17, 19] respectively. These Eu^{3+} sharp excitation bands indicate that violet and blue laser diodes/LEDs are efficient pumping sources to obtain a red emission from Eu^{3+} doping, which could be useful for white light devices. Furthermore, it is worthy to notice that the main difference between the samples in these two different formulas deals with the excitation intensities of the 4f-4f transitions of Eu^{3+}. The excitation band intensity of the $Ca_{1-x}Eu_xAl_2Si_2O_{8+0.5x}$ samples starts to decrease for a concentration beyond 10% (Figure 7, right), whereas it gradually increases (up to 13%) for the $C_{1-3x/2}Eu_xAl_2Si_2O_8$ formula.

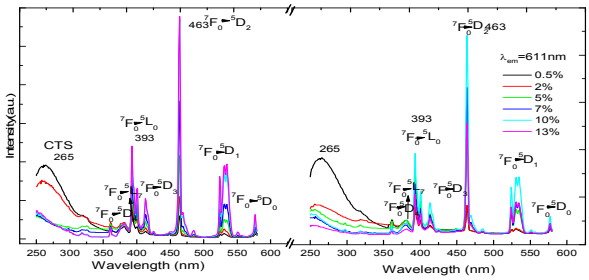

Figure.7 Left, excitation spectra of $C_{1-3x/2}ASO$: xEu^{3+} and right, excitation spectra of $C_{1-x}ASO_{8+0.5x}$: xEu^{3+} (x = 0.5% to 13%), monitored at 611 nm

Figure 8 shows the emission spectra of the samples $C_{1-3x/2}Eu_xAl_2Si_2O_8$ and $Ca_{1-x}Eu_xAl_2Si_2O_{8+0.5x}$ (x = 0.5% to 13%) monitored at 463 nm ($^5D_0 \rightarrow ^7F_2$, predominant transition of Eu^{3+}) for different Eu concentrations (the insets show the peaks of the Eu^{3+} $^5D_0 \rightarrow ^7F_2$ transitions). For each composition, the strongest emission peak is located at 611 nm and attributed to the $^5D_0 \rightarrow ^7F_2$ transition. Other peaks located at 570-579, 580-604, 638-661and 679-715 nm are assigned to the $^5D_0 \rightarrow ^7F_0$, $^5D_0 \rightarrow ^7F_1$, $^5D_0 \rightarrow ^7F_3$ and $^5D_0 \rightarrow ^7F_4$ transitions of the Eu^{3+} ions, [17, 19] respectively. As the red emission generated from the $^5D_0 \rightarrow ^7F_2$ transition predominates in the emission spectra, one can suppose that Eu^{3+} cations occupy sites having no inversion centre in the CASO matrix, as expected for Eu housed in both the 6-fold Ca1 and 7-fold Ca2,3,4 sites. As previously seen for excitation spectra, similarly, a quenching of Eu^{3+} emission can be also only observed for the $C_{1-x}Eu_xAl_2Si_2O_{8+0.5x}$ formula when the doping rate reaches 10%. Therefore, one can suppose that for the same doping rate, $C_{1-3x/2}Eu_xAl_2Si_2O_8$ samples contain less Eu^{3+} ions than samples under the other formula and consequently, the $C_{1-3x/2}Eu_xAl_2Si_2O_8$ samples would have more

Eu^{2+} ions than in the $C_{1-x}Eu_xAl_2Si_2O_{8+0.5x}$ for a given Eu concentration.

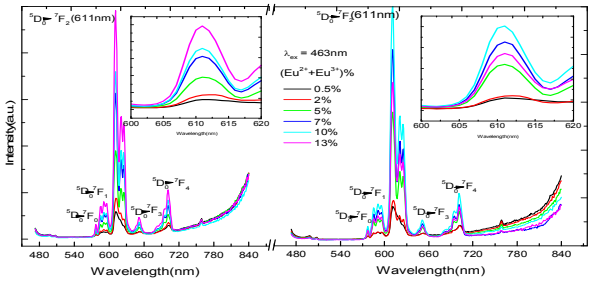

Figure.8 (Left) emission spectra of $C_{1-3x/2}ASO$: xEu^{3+}, and (right) emission spectra of $C_{1-x}ASO$: xEu^{3+} (x = 0.5% to 13%), excited at 463 nm

3.3. Mechanism of the "abnormal" reduction from Eu^{3+} to Eu^{2+}

Commonly, it is well accepted that the stabilization of Eu^{2+} cations is triggered in reducing conditions, while Eu^{3+} cations are naturally stabilized in air or in pure oxygen. From this postulate, the reciprocal is often deduced, that synthesis in air will conduct systematically to the stabilization of Eu^{3+} cations only, while the use of Ar/H_2 atmosphere will lead to the systematic reduction of Eu^{3+} into Eu^{2+}. In fact, such assertions have to be modulated as discussed below. In this section, we try to determine the mechanism about the "abnormal" reduction of Eu^{3+} to Eu^{2+} occurring in the CASO when synthesised in air condition with Eu^{3+} containing precursors as Eu_2O_3. We do here the hypothesis that Eu^{3+} cations are first inserted in the matrix, and that the latter reorganizes its composition to favour the appearance of Eu^{2+} ions. In principle, the reduction of Eu^{3+} cations into Eu^{2+} ones require electron transfers from chemical elements of the host lattice towards the rare earth. In the CASO matrixes, no element can be reduced. Thus, we may wonder where the electrons come from and how they are transferred to the doped Eu^{3+} ions in the CASO matrix. From a chemistry point of view, when dopant is inserted in place of alkaline earth elements under the divalent state (Eu^{2+}), overall charge compensation in the CASO lattice is fulfilled by a one to one substitution (Ca^{2+}-Eu^{2+}). In contrast, for Eu^{3+} cations at the Ca^{2+} sites, charge compensation requires changing in composition of the host lattice, which is appearance of cationic vacancies or oxygen atoms at interstitial sites. These two types of charge rearrangements can be schematized as followed:

$3Ca^{2+} = 2Eu^{3+}_{Ca} + V_{Ca^{2+}}$ (under formulation $Ca_{1-3x/2}Eu_xAl_2Si_2O_8$)

$3Ca^{2+} = 2Eu^{3+}_{Ca} + Ca^{2+} + O_i^{2-}$ (under formulation $Ca_{1-x}Eu_xAl_2Si_2O_{8+0.5x}$)

For the former case, one alkaline earth vacancy defect V''_{Ca} with two negative charges is generated as well as two substituting defects with a net +1 charge. In some extent, we can regard one vacancy V''_{Ca} (with two negative charges) as an electron donor and similarly, the two positive $Eu^{\bullet}_{Ca}$ defects as electron acceptors. As a result, under thermal stimulus, the negative charges of the vacancy defects V''_{Ca} would be transferred to the Eu^{3+} sites and reduce them to the divalent state. The whole process can be expressed by the following Equation (2):

$$2[Eu_{Ca}]^{\bullet} + [V_{Ca}]'' = 2[Eu_{Ca}]^{x} + [V_{Ca}]^{x} \quad (2)$$

By considering this model, highly used in the glass community, [34] we can suppose if more V''_{Ca} are created, more Eu^{3+} ions will be present, and higher will be their propensity to be reduced into the divalent state. Based on this postulate, more vacancies are created in $Ca_{1-3x/2}Eu_xAl_2Si_2O_8$ sample than in $Ca_{1-x}Eu_xAl_2Si_2O_{8+0.5x}$ one for identical Eu dopant concentrations. Consequently, more Eu^{2+} cations are expected to be stabilized in $Ca_{1-3x/2}Eu_xAl_2Si_2O_8$ than in $Ca_{1-x}Eu_xAl_2Si_2O_{8+0.5x}$ at a given Eu concentration which are in good agreement with the observations (Figures 7 and 8).

To further confirm the hypothesis that an increase of V''_{Ca} in the CASO matrix would facilitate the reduction from Eu^{3+} to Eu^{2+}, we also prepared a series of materials with different co-dopants in the CASO series and analyse their optical properties. The chosen co-dopants were K^+, La^{3+} and Zr^{4+}. Materials were prepared in the same conditions as reported for CASO: $Eu^{2+/3+}$ in air condition. In this context, we prepared $Ca_{0.90}Eu_{0.05}K_{0.05}Al_2Si_2O_8$ (0 V''_{Ca} per Eu atom), $Ca_{0.85}Eu_{0.05}La_{0.05}Al_2Si_2O_8$ (1 V''_{Ca} per Eu atom) and $Ca_{0.825}Eu_{0.05}Zr_{0.05}Al_2Si_2O_8$ (1.5 V''_{Ca} per Eu atom) compounds compared with the "un-codoped" compound $Ca_{0.925}Eu_{0.05}Al_2Si_2O_8$ (0.5 V''_{Ca} per Eu atom). As $r(K^+) = 1.37$ Å when $CN = 6$ and 1.38 Å when $CN = 7$, $r(La^{3+}) = 1.032$ Å when $CN = 6$ and 1.10 Å when $CN = 7$, $r(Zr^{4+}) = 0.72$ Å when $CN = 6$ and 0.78 Å when $CN = 7$, all these ions are more likely to replace the Ca^{2+} ions in the CASO matrix for steric reason as usual. Figure 9 displays the photoluminescence spectra of the four materials ($\lambda_{ex} = 393$ nm) while Table 2 reports information related to the nature of the substitution and the intensity ratio between Eu^{2+} and Eu^{3+}. In this table, R is defined as the ratio of the number of effective electrons on negative defects (total negative net charge on defects) and the number of expected Eu^{3+} ions to be reduced.

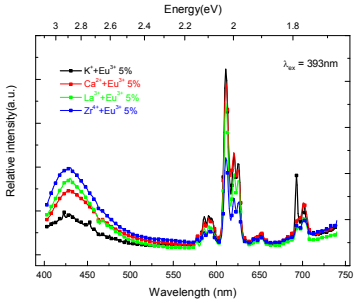

Figure.9 Emission spectra of co-doped samples of CASO: $0.05Eu^{3+}$, $0.05M^{n+}$ from which the $I(Eu^{2+}/Eu^{3+})$ in Table 2 was calculated, monitored at $\lambda_{ex} = 393$nm.

Table 2 Evolution of the Eu^{2+}/Eu^{3+} intensity ratio versus the number of V_{Ca} vacancies per Eu in $Ca_{0.90}Eu_{0.05}M_{0.05}Al_2Si_2O_8$ materials

Substitution reaction	Positive defect	Negative defect	$R^{(a)}$	$I(Eu^{2+}/Eu^{3+})^{(b)}$
$2\,Ca^{2+} \rightarrow Eu^{3+} + K^{+}$ (0 $V_{Ca}^{//}$ /Eu)	$[Eu_{Ca}]^{\bullet}$	$[K_{Ca}]^{/}$	≤1/1=1	0.216
$3Ca^{2+} \rightarrow 2Eu^{3+} + V_{Ca}$ (0.5 $V_{Ca}^{//}$ /Eu)	$2[Eu_{Ca}]^{\bullet}$	$[V_{Ca}]^{//}$	2/2=1	0.287
$3Ca^{2+} \rightarrow Eu^{3+} + La^{3+} + V_{Ca}$ (1 $V_{Ca}^{//}$ /Eu)	$[Eu_{Ca}]^{\bullet}$ $[La_{Ca}]^{\bullet}$	$[V_{Ca}]^{//}$	2/1=2	0.374
$7Ca^{2+} \rightarrow 2Eu^{3+} + 2Zr^{4+} + 3V_{Ca}$ (1.5 $V_{Ca}^{//}$ /Eu)	$2[Eu_{Ca}]^{\bullet}$ $2[Zr_{Ca}]^{\bullet\bullet}$	$3[V_{Ca}]^{//}$	6/2=3	0.8995

(a) *R* is ratio of the number of effective electrons on negative defects and the number of Eu^{3+} ions to be reduced and (b) is the intensity ratio between Eu^{2+} and Eu^{3+} ($I_{max}Eu^{2+}/I_{max}Eu^{3+}$)

As shown in Figure 9, it appears that the intensity of the Eu^{2+}-5d → 4f transition increases along the K, Ca, La, Zr sequence. At the opposite, the inverse trend is observed for the evolution of the intensity of the Eu^{3+}-4f → 4f transitions. Meanwhile, according to the results reported in Table 2, the increase of *R* favours the reduction from Eu^{3+} to Eu^{2+}. Namely, following the sequence $K^{+} < Ca^{2+} < La^{3+} < Zr^{4+}$, the ratio of initial Eu^{3+} ions which undergoes a reduction increases. Let notice here depletion of the $V_{Ca}^{//}$ quantity at the benefit of the appearance of Eu^{2+} may be temperature dependant. Namely, we may envision a thermo stimulated phenomenon which favours the hoping of an electron from the vacancy towards a Eu^{3+} site following the temperature. To confirm this hypothesis, we also measured the emission intensities generated from $Eu^{2+/3+}$ in the $C_{1-3x/2}Eu_xAl_2Si_2O_8$ (x = 10%) under different temperatures. As one can see Figure 10, the emission intensities from the Eu^{3+} decreases when the temperature increases while the emission intensities associated with Eu^{2+} is enhanced. Obviously, this phenomenon can be explained by changing in the different amount of Eu^{2+} (increasing) and Eu^{3+} (decreasing) ions in the $C_{1-3x/2}Eu_xAl_2Si_2O_8$ following the temperature.

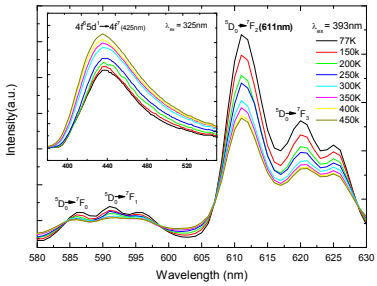

Figure.10 Temperature dependence of emission spectra for $C_{1-3x/2}Eu_xASO$ (x = 10%) sample under λ_{ex} = 393 nm. The inset shows the relative intensity of the same sample under λ_{ex} = 325 nm

3.4. Mechanism of ET from Eu^{2+} to Eu^{3+}

Based on above experimental results, the energy level diagram of Eu^{2+} and Eu^{3+} ions and its possible pathway for the ET from Eu^{2+} to Eu^{3+} ions are schematically drawn in Figure S5. In this study, we measured the luminescent properties of the Eu^{3+} corresponding to the transitions from the lowest excited $^5D_0$ level to ^7F_j levels under the excitation corresponding to the $^7F_0 \rightarrow {}^5D_2$ transition. As previously observed, the luminescence is associated with the non-radiative relaxation of the excited Eu^{3+} ion in the higher excited states to the $^5D_0$ level and the radiative transition into the ground ^7F_j levels. Moreover, with the co-existence of Eu^{2+}, as one can see Figure S5, the emission spectra of the Eu^{2+} ($4f^65d^1$ (e_g) →$4f^7$) is overlapped with the excitation spectra of Eu^{3+} ($^7F_J \rightarrow {}^5D_4$, $^5D_3$ till $^5D_0$). Thus, the ET from Eu^{2+} to Eu^{3+} is considered as follows: the excited Eu^{2+} in the $4f^65d^1$ (e_g) level partly radiatively relaxes to the ground state $^8S_{7/2}$, and the rest part of the energy causes the excitation of Eu^{3+} ion.

Formally, ET can only occur if there is overlap between the emission spectrum of the sensitizer (Eu^{2+}) and the excitation spectrum of the activator (Eu^{3+}). [28, 35, 36] Such a condition is respected as depicted in Figure 11. Figure S6 represents the excitation spectra for Eu doped CASO prepared in air and reducing conditions, respectively. The emission of Eu^{2+} cations only at around 425 nm is triggered by excitation of CASO: Eu at 287 and 320 nm. Clearly, the excitation spectrum of CASO: $Eu^{2+/3+}$ monitored at 611 nm, i.e. a characteristic lines of Eu^{3+} 4f-4f transitions, evidences a peak at 320 nm. Consequently, we can conclude that we can induce emission of Eu^{3+} via the excitation of Eu^{2+}, what imply ET from Eu^{2+} cations towards Eu^{3+} ones. This is also asserted via the collect of the excitation spectrum of CASO: Eu prepared in reducing atmosphere (containing slight amount of Eu^{3+} cations) when monitored at 611 nm (Figure S3). At the end, the variation of the decay times collected for CASO: $Eu^{2+/3+}$ samples also agree with ET as shown below.

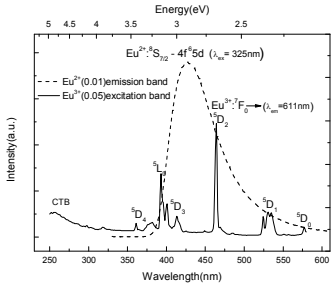

Figure.11 Overlap of Eu^{2+} luminescence spectrum (λ_{ex} = 320nm) with Eu^{3+} excitation spectrum for CASO matrix as-prepared Eu-doped samples under formula $C_{1-3x/2}ASO:xEu^{3+}$ (x = 0.05) and $C_{1-x}ASO: xEu^{2+}$ (x = 0.01)

The room-temperature decay curves are shown in Figure S7 for x ranging from 0.5% to 13%. In contrast to CASO: Eu^{2+} prepared in reducing atmosphere (Figure 6) where lifetime remains constant whatever the Eu concentrations, we notice here a decrease of τ from 0.65 µs to 0.26 µs going from $Ca_{0.9925}Eu_{0.005}Al_2Si_2O_8$ to $Ca_{0.805}Eu_{0.13}Al_2Si_2O_8$. Again, this suggests some ET from Eu^{2+} to Eu^{3+}. The same observation can be also done for $C_{1-x}Eu_xASO_{8+0.5x}$ compositions (Figure S7 and Table 3).

Table 3 Lifetimes of the emission decay of Eu^{2+} (monitored at 420nm) in the two groups of samples

Eu concentration	$C_{1-x}Eu_xASO_{8+0.5x}$	$C_{1-3x/2}Eu_xASO$
0.5%	0.65 µs	0.65 µs
2%	0.64 µs	0.64 µs
5%	0.52 µs	0.58 µs
7%	0.42 µs	0.53 µs
10%	0.32 µs	0.40 µs
13%	0.26 µs	0.29 µs

Generally, the ET efficiency from a sensitizer (Eu^{2+}) to activator (Eu^{3+}) can be expressed by the following Equation (3): [28, 33]

$$\eta_T = 1 - \frac{I_S}{I_{S0}} \approx 1 - \frac{\tau_S}{\tau_{S0}} \qquad (3)$$

where τ_s and τ_{s0} are the decay lifetimes of the sensitizer (Eu^{2+}) in the presence and absence of the activator (Eu^{3+}), respectively. Here, τ_{s0} is the intrinsic decay time of Eu^{2+} emission when CASO is only doped by Eu^{2+}, namely 0.65 µs. τ_s is the decay time of the sensitizer (Eu^{2+}) in the presence of an activator (Eu^{3+}), i.e. the decay times of Eu^{2+} of samples prepared in air. The collected values are expressed in Table 3. Thus, the ET efficiency of Eu^{2+}-Eu^{3+} in CASO host lattice is calculated for the samples under the different formulations (Figure 12). The η_T increases gradually with Eu concentration. Moreover, η_T is systematically higher for $C_{1-3x/2}Eu_xAl_2Si_2O_8$ than $C_{1-x}Eu_xAl_2Si_2O_{8+0.5x}$ for a given x value due to the different ratio of the Eu^{2+}/Eu^{3+}.

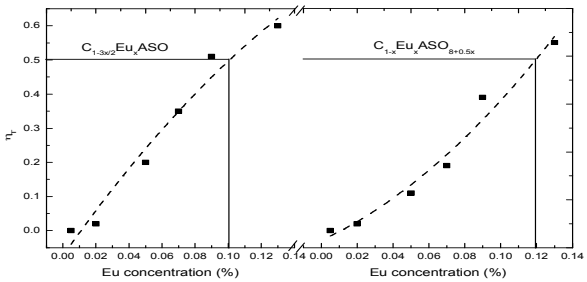

Figure.12 ET efficiencies for Eu^{2+} to Eu^{3+} under the formula $C_{1-3x/2}Eu_xASO$ (left) and $C_{1-x}Eu_xASO_{8+0.5x}$ (right), x = 0.5% to 13%

The average separation R (Eu^{2+}-Eu^{3+}) can be expressed by Equation (3), [28,42,43]

$$R_C = 2\left[\frac{3V}{4\pi X_c N}\right]^{1/3} \qquad (3)$$

where R corresponds to the mean separation between the nearest Eu^{2+} and Eu^{3+} ions at the critical concentration, x is the total concentration of Eu^{2+} and Eu^{3+}. Thus, R (Eu^{2+}-Eu^{3+}) (in Å) were determined to be 40.00, 25.20, 18.57, 16.60, 14.74 and 13.50 corresponding to x = 0.005, 0.02, 0.05, 0.07, 0.1 and 0.13, respectively, in both of the two groups of samples. The critical concentrations at which the ET efficiency fixed at 0.5 [36] are about 0.102 and 0.120 under the formula $C_{1-3x/2}Eu_xAl_2Si_2O_8$ and $C_{1-x}Eu_xAl_2Si_2O_{8+0.5x}$, respectively (Figure 12). Thus, if we define that the critical concentration x_c is the concentration at while η_T equal 0.5, the critical distance (R_c) of the ET is calculated to be ~ 14.64Å and 13.87Å for $C_{1-3x/2}Eu_xAl_2Si_2O_8$ and $C_{1-x}Eu_xAl_2Si_2O_{8+0.5x}$, respectively. The resonant ET mechanism consists of two types: 1) exchange interaction and 2) multipolar interaction. It is known that if ET belongs to the exchange interaction, the critical distance between the sensitizer and activator should be shorter than ~ 5 Å. [5, 37] In our case, the critical distance between Eu^{2+} and Eu^{3+} are 14.64 and 13.87 Å under the two different formulas, respectively. Therefore, the ET mechanism should be under the second case in this study, namely, multipolar interaction. Furthermore, the ET mechanism between Eu^{2+} and Eu^{3+} in $C_{1-3x/2}Eu_xAl_2Si_2O_8$ and $C_{1-x}Eu_xAl_2Si_2O_{8+0.5x}$ are controlled by electric multipole-multipole interactions according to Dexter theory, [28, 33, 35, 36] which follows the ET Equation (4) given below:

$$\frac{\tau_{S0}}{\tau_S} \propto C^{a/3} \qquad (4)$$

where τ_{S0} and τ_S are the luminescence decay times of Eu^{2+} cations in the absence and presence of Eu^{3+}, respectively. C is the sum of Eu^{2+} and Eu^{3+} contents. The a parameter equals to 6, 8 and 10 corresponding to dipole-dipole, dipole-quadrupole and quadrupole-quadrupole interactions, respectively. The τ_{S0}/τ_S vs. $C^{a/3}$ curves are represented in Figure 13a and Figure 13b for the $C_{1-3x/2}Eu_xAl_2Si_2O_8$ and $C_{1-x}Eu_xAl_2Si_2O_{8+0.5x}$ formulations, respectively. As shown in Figure 13, these curves indicate that the ET from Eu^{2+} to Eu^{3+} occurs rather via a dipole-dipole mechanism under the formula $C_{1-3x/2}Eu_xAl_2Si_2O_8$ and dipole-quadrupole mechanism under the formula $C_{1-x}Eu_xAl_2Si_2O_{8+0.5x}$. At this stage, we do not fully understand why the dipole-quadrupole mechanism is not obtained for both groups of samples as expected. Supplementary experiments are needed in progress to address this observation.

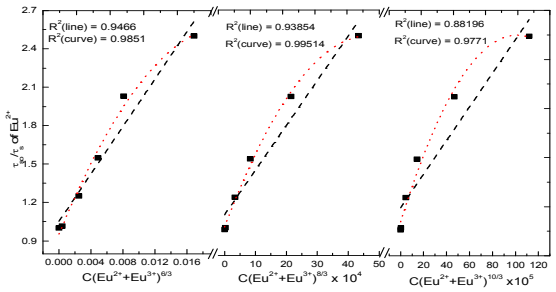

Figure.13a. Dependence of τ_{S0}/τ_S of Eu^{2+} on a) a = 6, b) a = 8 and c) a = 10 for the samples under the formula $C_{1-3x/2}Eu_xASO$, x = 0.5% to 13% (from left to right)

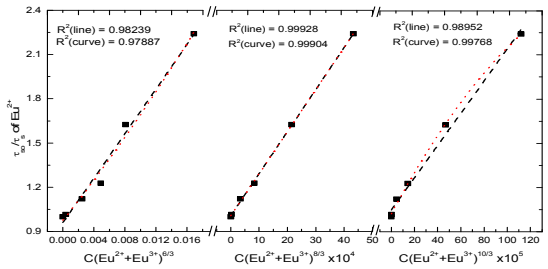

Figure.13b. Dependence of τ_{S0}/τ_S of Eu^{2+} on a) a = 6, b) a = 8 and c) a = 10 for the samples under the formula $C_{1-x}Eu_xASO_{8+0.5x}$, x = 0.5% to 13% (from left to right)

Conclusions

In summary, we have demonstrated the possibility to "co-dope" $CaAl_2Si_2O_8$ aluminosilicates host lattices by both Eu^{3+} and Eu^{2+} via high temperature solid-state reactions in air. The "only" Eu^{2+}-doped $CaAl_2Si_2O_8$ has to be prepared in reducing atmosphere. These materials, with a very low concentration of residual Eu^{3+} cations exhibit a bluish white luminescence centred at around 425 nm due to the allowed $4f^65d^1 \rightarrow 4f^7$ ($^8S_{7/2}$) radiative transition. For materials prepared in air, Eu^{2+} and Eu^{3+} cations coexist. In addition, the concentration of Eu^{2+} at the expense of Eu^{3+} cations can be privileged via the co-doping with a M^{x+}cation (Zr^{4+} for instance). This could open up the door to the synthesis of Eu^{2+} containing phosphors in air in the next future. As expected, the position and shape of the Eu^{3+} emission bands are not impacted by the nature of host lattice. For CASO composition, the strongest f-f emission peaks located at around 611 nm are attributed to the $^5D_0 \rightarrow {}^7F_2$ transition and can be sensitized by energy transfer from Eu^{2+}. This lead to the addition of red contribution to the bluish one observed for only Eu^{2+} doped materials. We expected to take benefit of these observations to generate new phosphors in the future with a control of the CIE (x, y) parameter and to tune white emission from cold to warm.

Acknowledgements

The authors acknowledge S. Jobic, P. Deniard, H. Serier-Brault and F. Massuyeau for the technical assistance and fruitful discussion in IMN, Nantes University, CNRS, FRANCE. This work has been supported by the Chinese Scholarship Council (CSC), NO. 2009615018.

Notes and references

[a] Institut des Matériaux Jean Rouxel, Université de Nantes, CNRS, 2 rue de la Houssinière, BP 32229, 44322 Nantes cedex 03, France.

[b] Institut Européen de Chimie et Biologie, IECB, UMR5248, Université Bordeaux 1, CNRS, France.

† Corresponding author, E-mail: wubin.dai@foxmail.com, fax: + 86 20 87 11 02 73.

1. V. Bachmann, C. Ronda, O. Oeckler, W. Schnick and A. Meijerink, *Chem. Mater.*, 2008, 21, 316-325.
2. F. Clabau, X. Rocquefelte, S. Jobic, P. Deniard, M.-H. Whangbo, A. Garcia and T. Le Mercier, *Solid State Sci.*, 2007, 9, 608-612.
3. F. Clabau, A. Garcia, P. Bonville, D. Gonbeau, T. Le Mercier, P. Deniard and S. Jobic, *J. Solid State Chem.*, 2008, 181, 1456-1461.
4. G. Denis, P. Deniard, E. Gautron, F. Clabau, A. Garcia and S. Jobic, *Inorg. Chem.*, 2008, 47, 4226-4235.
5. J. K. Park, J. M. Kim, E. S. Oh and C. H. Kim *Electrochem. Solid-State Lett.*, 2005, 8, H6-H8.
6. S. M. Lee and K. C. Choi, *Opt. Express*, 2010, 18, 12144-12152.
7. T. Kida, M. M. Rahman and M. Nagano, *J. Am. Ceram. Soc.*, 2006, 89, 1492-1498.
8. X. Y. Chen, Z. Li, S. P. Bao and P. T. Ji, *Opt. Mater.*, 2011, 34, 48-55.
9. F. Clabau, X. Rocquefelte, S. Jobic, P. Deniard, M. H. Whangbo, A. Garcia and T. Le Mercier, *Chem. Mater.*, 2005, 17, 3904-3912.
10. M. Peng and G. Hong, *J. Lumin.*, 2007, 127, 735-740.
11. M. L. Debasu, D. Ananias, A. G. Macedo, J. Rocha and L. s. D. Carlos, *J. Phys. Chem. B*, 2011, 115, 15297-15303.
12. T. Endo, T. Masuda, H. Takizawa and M. Shimada, *J. Mater. Sci. Lett.*, 1992, 11, 1330-1332.
13. S. A. Lourenço, N. O. Dantas, E. O. Serqueira, W. E. F. Ayta, A. A. Andrade, M. C. Filadelpho, J. A. Sampaio, M. J. V. Bell and M. A. Pereira-da-Silva, *J. Lumin.*, 2011, 131, 850-855.
14. Z. Pei, Q. Zeng and Q. Su, *J. Phys. Chem. Solids*, 2000, 61, 9-12.
15. C.-C. Wu, K.-B. Chen, C.-S. Lee, T.-M. Chen and B.-M. Cheng, *Chem. Mater.*, 2007, 19, 3278-3285.
16. A. Cho, S. Y. Kim, M. Lee, S.-J. Kim, C.-H. Kim and C.-H. Pyun, *J. Lumin.*, 2000, 91, 215-221.
17. M. D. Chambers, P. A. Rousseve and D. R. Clarke, *J. Lumin.*, 2009, 129, 263-269.
18. G. Blasse, *Chem. Mater.*, 1989, 1, 294-301.
19. G. Seeta Rama Raju, H. C. Jung, J. Y. Park, B. K. Moon, R. Balakrishnaiah, J. H. Jeong and J. H. Kim, *Sens. Actuators, B: Chem.*, 2010, 146, 395-402.
20. Y.-C. Chang, C.-H. Liang, S.-A. Yan and Y.-S. Chang, *J. Phys. Chem. B*, 2010, 114, 3645-3652.
21. S. Sapru and K. L. Tan, *physica status solidi (b)*, 1984, 125, K161-K163.
22. Z. W. P. Q. H. Zeng, S. B. Wang, Q. Su *Spectrosc. Lett.*, 1999, 32, 895.
23. C. Zhang, J. Yang, C. Lin, C. Li and J. Lin, *J. Solid State Chem.*, 2009, 182, 1673-1678.
24. M. Nogami, T. Yamazaki and Y. Abe, *J. Lumin.*, 1998, 78, 63-68.
25. J. Hao and M. Cocivera, *Appl. Phys. Lett.*, 2001, 79, 740-742.
26. J. Hao and M. Cocivera, *Appl. Phys. Lett.*, 2002, 81, 4154-4156.
27. J. Hao, J. Gao and M. Cocivera, *Appl. Phys. Lett.*, 2003, 82, 2778-2780.

28. W.-J. Yang, L. Luo, T.-M. Chen and N.-S. Wang, *Chem. Mater.*, 2005, 17, 3883-3888.
29. W. Z. Gebert, *Kristallogr*, 1972, 135, 437.
30. V. D. Petricek, M.; Palatinus, L., *The Crystallographic Computing System JANA, 2006 Beta*, Academy of Sciences: Praha, Czeck Republic, 2006.
31. R. J. Angel, *Am. Mineral.*, 1988, 73, 1114.
32. R. D. Shannon, *Acta Crystallogr*, 1976, A32, 751.
33. S. H. Lee, J. H. Park, S. M. Son, J. S. Kim and H. L. Park, *Appl. Phys. Lett.*, 2006, 89, -.
34. E. Malchukova and B. Boizot, *Mater. Res. Bull.*, 2010, 45, 1299-1303.
35. C.-H. Huang, T.-M. Chen, W.-R. Liu, Y.-C. Chiu, Y.-T. Yeh and S.-M. Jang, *ACS. Appl. Mater. Interfaces.*, 2010, 2, 259-264.
36. N. Guo, Y. Huang, H. You, M. Yang, Y. Song, K. Liu and Y. Zheng, *Inorg. Chem.*, 2010, 49, 10907-10913.
37. G. B. C. Blasse. G, *Luminescent Materials*, Springer-Verlag, 1994.